Advances in Continuous and Discrete Models

RESEARCH Open Access

Spatiotemporal patterns in a predator–prey model with anti-predation behavior and fear effect

Minghao Yang[1], Changcheng Xiang[1*] and Yi Yang[2]

*Correspondence:
xcc7426681@126.com
[1]School of Mathematics and Statistics, Hubei Minzu University, Enshi 445000, Hubei, China
Full list of author information is available at the end of the article

Abstract

In this study, a predator–prey model incorporating prey's fear effect and anti-predation behavior has been developed. The functional response takes the square root of the prey population and adds the predator's loss term. We prove the existence of the system's equilibrium point and derive the conditions for its local stability, as well as discuss how diffusion affects the system's stability. Bifurcation analysis of the parameters reveals that the fear effect leads to a decrease in the predator population in the coexistence equilibrium. In addition, we apply the finite difference method and the finite element method to simulate the diffusion model in rectangles and irregular customized regions, respectively. The results demonstrate that the system can eventually reach a uniform stable state after experiencing oscillations and fluctuations at certain parameters and initial values.

Keywords: Predator–prey model; Anti-predation behavior; Fear effect; Spatiotemporal pattern

1 Introduction

Since Lotka and Volterra [1, 2] pioneered the study of the predator–prey ecosystem, a large variety of models have been proposed to describe the interaction among species in the natural world. In fact there are various factors that affect the predator–prey system's dynamic behavior, such as environmental carrying capacity, the predator's foraging efficiency, the prey's reproductive rate, and so on. In order to describe the relationship among the species, the scholars have successively established various research models incorporating various forms of functional responses, such as Holling I–IV types [3–5], Beddington–DeAngelis functional response [6, 7], ratio-dependent functional response [8], Crowley–Martin functional response [9, 10], etc.

Observations of social animals in grasslands revealed that predators tend to target weaker prey first during hunts. Therefore, stronger prey individuals will encircle and protect the weaker members in the center to avoid predation. For instance, elephants will form a defensive circle to protect the baby elephants from lion attacks. In [11], the authors first proposed the square root functional response to simulate this defensive strategy based on

the situation of the herbivores populating the savannas and their large predators, the prey adopt a circular defensive strategy, with predator–prey interactions occurring on the outer periphery of the prey group. Braza [12] studied a more general model with square root functional response, which effectively represents systems where the prey demonstrates strong herd structure. They used $\frac{\sqrt{u}v}{1+\alpha\sqrt{u}}$ as the functional response in order to describe the predator–prey reaction between some animals that take circular defensive strategy. Tang [13] introduced spatial diffusion on the basis of Ajraldi's [11] model and studied the dynamics of the diffusive predator–prey model with herd behavior. Panja [14] supposed that the prey populations have herd behavior and prey refuges, considered the square root functional response and prey refuge behavior in their proposed model to study the joint effects of these two parameters in the population dynamics.

Due to their habit of living in groups, the weaker members of the prey in the center are shielded by the adult prey on the periphery of the protective ring, which also indicates that adult prey have a certain level of aggression. Especially in grassland animals, prey always try to avoid predation by fighting or running away, some aggressive prey species can sometimes attack or even kill predators when they resisting predation, such as buffalo, porcupine, and giraffe. In certain scenarios, adult prey may engage in attacks against juvenile predators as a means of mitigating future predation pressure [15]. To account for this anti-predation behavior, we use a predator loss term in our model. Animals will always respond to perceived predation risks and show a variety of biological behaviors, such as migratory behavior, foraging reduction, psychological changes [16, 17]. For instance, when a species is frightened by predators, it is less likely to go out for food, which reduces birth and survival rates [18]. In order to escape predation, prey may migrate to low-risk areas, which increases the cost of survival and leads to a decline in the population [16]. In the wild, it is easy to observe that the death of prey is due to the attack of predators [19], but several studies have shown that in some prey species, the fear effect indirectly affects prey birth even more than direct predation [20]. Recently, Wang et al. [21] investigated a general predator–prey model with fear effect and considered anti-predation defensive behavior as a cost that affected prey birth. As the predator's attack intensity increases, the animals will mount stronger anti-predation defences. Taking $\frac{1}{1+kv}$ as the fear effect term and introducing the mature delay makes the predator–prey system more complex [22]. Samaddar [23] studied how the presence of fear effect re-calibrated the effects of prey refuge and additional food in terms of quality and quantity on the system dynamics.

In the real world, predatory behavior in nature is often accompanied by population diffusion due to factors such as water, food availability, and climate. Predator and prey tend to move from high-density areas to low-density areas in response to resource distribution, invasion of natural enemies, and natural disasters [24]. Turing [25] pioneered the idea that the population diffusion would affect the stability of the system under certain conditions. In 1972, Segel and Jackson [26] extended the reaction–diffusion equation to the biomathematical model. The solutions of reaction–diffusion equations display a wide range of behaviors, including traveling waves, stripes, spiral patterns, and chaos [27]. Through mathematical analysis and numerical simulations, Guin [28] displays a parametric Turing space where various spatiotemporal patterns, namely stripes, spots, spot–stripe mixture patterns, emerge. Souna [29] proved the existence of diffusion driven instability at the positive equilibrium point in a diffusive predator–prey model with social behavior. The biological reaction diffusion systems have become one of the most dominant themes

in mathematical biology, and there have been abundant research works on them so far; the readers could refer to [13, 30–35].

In the remainder of this paper, we investigate a predator–prey model incorporating diffusion, grounded in the aforementioned biological behavior of group anti-predation and analyze the dynamics of the model such as existence, stability, and bifurcation. Then we perform numerical simulations using finite difference and finite element methods, respectively, which support and extend the theoretical results.

2 Mathematical model and the existence of equilibrium point

Based on the above biological characteristics, we propose a coupled reaction–diffusion model with anti-predation behavior and fear effect as follows:

$$\begin{cases} \frac{\partial u(x,t)}{\partial t} = \frac{u}{1+bv} - \frac{u^2}{r} - \frac{m\sqrt{u}v}{\sqrt{u}+c} + d_1\Delta u, & x \in \Omega, t > 0, \\ \frac{\partial v(x,t)}{\partial t} = -\beta v + \frac{\alpha m\sqrt{u}v}{\sqrt{u}+c} - \eta uv + d_2\Delta v, & x \in \Omega, t > 0, \\ \frac{\partial u}{\partial \boldsymbol{n}} = \frac{\partial v}{\partial \boldsymbol{n}} = 0, & x \in \partial\Omega, t > 0, \\ u(x,0) = u_0(x) \geq 0, v(x,0) = v_0(x) \geq 0, & x \in \Omega. \end{cases} \tag{1}$$

Here, u and v denote, respectively, the prey and predator populations at time t and $\Delta = \sum_{i=1}^{n} \frac{\partial^2}{\partial x_i^2}$ $(n = 1, 2)$ is the Laplacian operator in space Ω, where Ω represents a suitable spatial domain in one or two dimensions. $\boldsymbol{n}$ is the outward unit normal vector of the boundary $\partial\Omega$, d_1, d_2 are diffusion coefficients of the prey and predator populations, respectively. We assume that system (1) is subjected to the homogeneous Neumann boundary condition, which means that the species cannot leave the domain Ω and there is also no outside species entering Ω. The parameter r stands for the carrying capacity of the environment for prey species, b designates the fear effect, m is the capturing rate of predator, and c denotes the interference coefficient of the predator. The parameter α is the conversion rate of prey to predator and β is the death rate of the predator. η denotes the prey's resistance to predation, typically a very small value. The above parameters in the model are assumed to be positive.

This model describes the predation of two species in a closed space, $\frac{1}{1+bv}$ is used to represent the role of the fear effect, the presence of a greater number of v results in a reduced birth rate for the u. Because of the anti-predation behavior of prey, the response function is represented by $\frac{\sqrt{u}v}{\sqrt{u}+c}$. The aggression and resistance of the prey result in the loss of the predator, denoted by ηuv. d_1, d_2 reflect the diffusion rate of the two species respectively, $d_1 = d_2 = 0$ indicates that both prey and predator are sedentary, i.e., there is no diffusion, we have the following ODE system:

$$\begin{cases} \frac{du(t)}{dt} = \frac{u}{1+bv} - \frac{u^2}{r} - \frac{m\sqrt{u}v}{\sqrt{u}+c}, \\ \frac{dv(t)}{dt} = -\beta v + \frac{\alpha m\sqrt{u}v}{\sqrt{u}+c} - \eta uv. \end{cases} \tag{2}$$

It is noted that the equilibrium points of system (2) need to satisfy the following equation:

$$\begin{aligned} f(u,v) &= \frac{u}{1+bv} - \frac{u^2}{r} - \frac{m\sqrt{u}v}{\sqrt{u}+c} = 0, \\ g(u,v) &= -\beta v + \frac{\alpha m\sqrt{u}v}{\sqrt{u}+c} - \eta uv = 0. \end{aligned} \tag{3}$$

Clearly, system (2) has two boundary equilibria: the trivial equilibrium $P_0 = (0, 0)$ and the predator-free equilibrium $P_1(r, 0)$. Now we consider the internal equilibrium point $P^* = (u^*, v^*)$ with biological significance.

When $b = \eta = 0$, as the model considered in [12], there is an internal equilibrium point E^* if $\alpha m > \beta$ and $\frac{\beta c}{\alpha m - \beta} \leq r$, where

$$E^* = \left(\frac{\beta^2 c^2}{(\alpha m - \beta)^2}, \frac{\alpha m c^2 (r\beta^2 - c^2\beta^2 - 2\alpha\beta m r + \alpha^2 m^2 r)\beta}{rm(\alpha m - \beta)^4} \right). \tag{4}$$

Now we consider the aggression of prey and fear effects into the model, i.e., $b > 0$, $\eta > 0$. We have the following results on the existence of coexistence equilibrium.

Theorem 2.1 *System (2) has a positive equilibrium point if and only if the condition* Λ: $\alpha m > \beta, g(H^2, 1) \geq 0, u_1^* < r$ *holds, where* $H = \frac{\sqrt{c^2\eta^2 + 3\eta(\alpha m - \beta)} - \eta c}{3\eta} > 0$, u_1^* *is the smaller positive root of equation* $g(u, 1) = -\beta + \frac{\alpha m \sqrt{u}}{\sqrt{u} + c} - \eta u = 0$.

Proof We start with $g(u, v) = 0$, let $e = \sqrt{u}$ for convenience. Then, solving equation $g(u, v) = 0$ is equivalent to finding a solution e, it should satisfy:

$$G(e) = -\eta e^3 - \eta c e^2 + (\alpha m - \beta)e - \beta c = 0. \tag{5}$$

The function $G(e)$ is differentiable with respect to e, take the derivative of e:

$$G'(e) = -3\eta e^2 - 2\eta c e + \alpha m - \beta. \tag{6}$$

Since $G(0) < 0$ and the smaller solution of $G'(e) = 0$ is less than 0, in order to ensure that the maximum point of $G(e)$ is positive, $\alpha m > \beta$ is necessary, then $H = \frac{\sqrt{c^2\eta^2 + 3\eta(\alpha m - \beta)} - \eta c}{3\eta} > 0$ is the maximum point of $G(e)$ when $e > 0$. Let $g(H^2, 1) \geq 0$ such that $G(H) \geq 0$, thus $g(u, v) = 0$ has positive solutions. Next we consider $f(u, v)$. Define

$$F(e, v) = A_1 v^2 + A_2 v + A_3, \tag{7}$$

where $A_1 = mb$, $A_2 = \frac{be^4 + cbe^3}{r} + m$, $A_3 = \frac{e^4}{r} + \frac{ce^3}{r} - e^2 - ce$. Then

$$f(u, v) = 0 \Longleftrightarrow F(e, v) = A_1 v^2 + A_2 v + A_3 = 0.$$

It is obvious that $A_1 > 0$ and $A_2 < 0$ because all the parameters in model (1) are positive. There is a positive solution v of $F_{e=e^*}(v)$ if and only if $A_3 < 0$. Note that $A_3 \cdot \frac{r}{e} = (e - \sqrt{r})[e^2 + (c + \sqrt{r})e + \sqrt{r}c]$, therefore it is necessary for $u^* < r$ to ensure that $A_3 < 0$. Moreover, $v_* = \frac{\sqrt{A_2^2 - 4A_1A_3} - A_2}{2A_1} > 0$. □

As shown in Fig. 1, there may be two internal equilibrium points in the system when the loss term of the predator is considered in the model. When the equilibrium exists, the equilibrium value of the prey becomes higher than E^*. With the increase in the environmental capacity of prey, the population fluctuation of predator and prey increases, and it becomes more difficult to achieve a coexistence equilibrium. In addition, predators will

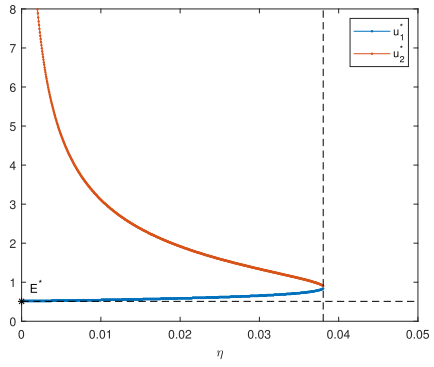

Figure 1 Values of prey u at coexistence equilibrium. The parameters are fixed as $\alpha = 0.78$, $\beta = 0.08$, $b = 1$, $c = 1$, $m = 0.3$, $r = 2.39$

suffer losses due to the anti-predation behavior of prey during the hunting process, therefore when the environmental carrying capacity of the prey is improved to a certain extent, i.e., the living environment is ideal enough, then the predators will struggle to survive and go extinct.

Remark 2.2 In a general predator–prey relationship, predator populations have always shown a positive increase when their food is plentiful, that is, relationship $\alpha m > \beta$ should always be true. When prey is less injurious and the prey's living environment is good enough for survival, the existence of a nontrivial equilibrium point for system (2) is ensured.

Remark 2.3 Assume that the condition $\wedge$ in Theorem 2.1 holds. There are two solutions to $g(u, 1) = 0$ when $g(H^2, 1) > 0$; without loss of generality, let us set $0 < u_1^* < u_2^*$. Since the analytical approach is similar, we will use u_1^* for numerical simulation later. To ensure the existence of an internal equilibrium point, we assume that the condition $\wedge$ holds throughout the remainder of this paper.

3 Stability and bifurcation analysis

In this section, we shall discuss the stability of the equilibrium points with and without diffusion by linearization and study the existence of Turing and Hopf bifurcation.

3.1 Stability of equilibrium state for ODE system (2)

The Jacobian of system (2) evaluated at an arbitrary equilibrium point $P(u, v)$ is given by

$$J = \begin{bmatrix} a_{11} & a_{12} \\ a_{21} & a_{22} \end{bmatrix},$$

where

$$\begin{aligned} a_{11} &= \frac{df}{du}(u, v) = \frac{1}{1 + bv} - \frac{2u}{r} - \frac{cmv}{2\sqrt{u}(\sqrt{u} + c)^2}, \\ a_{12} &= \frac{df}{dv}(u, v) = -\frac{ub}{(1 + bv)^2} - \frac{m\sqrt{u}}{\sqrt{u} + c}, \\ a_{21} &= \frac{dg}{du}(u, v) = \frac{\alpha cmv}{2\sqrt{u}(\sqrt{u} + c)^2} - \eta v, \end{aligned} \tag{8}$$

$$a_{22} = \frac{dg}{dv}(u,v) = -\beta + \frac{\alpha m\sqrt{u}}{\sqrt{u}+c} - \eta u.$$

Then the linear stability analysis at the equilibrium point of system (2) transforms into an eigenvalue problem for the Jacobian matrix J. The characteristic equation is

$$|J - \lambda I| = 0. \tag{9}$$

It is well known that the stability of the equilibrium point is equivalent to the condition where all the real parts of the eigenvalues are negative,

$$\lambda_i = \frac{T_1 \pm \sqrt{T_1^2 - 4D_1}}{2} < 0, i = 1,2,$$

where $D_1 = a_{11}a_{22} - a_{12}a_{21}$ and $T_1 = a_{11} + a_{22}$. We now present the following theorem concerning the stability of various equilibrium points when there is no diffusion.

Theorem 3.1 *For system* (2), (*i*) *the trivial equilibrium* $P_0(0,0)$ *is always an unstable saddle point*; (*ii*) *the predator-free equilibrium* $P_1(r,0)$ *is locally stable if* $u_2^* < r$ *and unstable if* $u_2^* \geq r$; (*iii*) *let* $e = \sqrt{u_1^*}$, *the positive equilibrium* $P^*(u^*,v^*)$ *is locally stable if the condition* $\frac{\eta v^*}{\alpha c} < \frac{mv^*}{2e(e+c)^2} < \frac{e^2}{r(2e+c)}$ *is satisfied*.

Proof The Jacobian matrix at $P_0(0,0)$ is given by $J_{(0,0)} = \begin{bmatrix} 1 & 0 \\ 0 & -\beta \end{bmatrix}$, implying the saddle nature of the equilibrium P_0. The Jacobian matrix corresponding to $P_1(r,0)$ is $J_{(r,0)} = \begin{bmatrix} a_1 & a_2 \\ a_3 & a_4 \end{bmatrix}$, where

$$a_1 = -1, a_2 = -br - \frac{m\sqrt{r}}{\sqrt{r}+c}, a_3 = 0, a_4 = -\beta + \frac{\alpha m\sqrt{r}}{\sqrt{r}+c} - \eta r.$$

Therefore, we need to ensure that $a_4 < 0$ so that $\det(J_{(r,0)}) > 0$, $\mathrm{tr}(J_{(r,0)}) < 0$. Under the given condition $\wedge$, it is evident from the proof of Theorem 2.1 that $g(u,1) = -\beta + \frac{\alpha m\sqrt{u}}{\sqrt{u}+c} - \eta u \geq 0$ only if $u_1^* < u < u_2^*$ when $u > 0$. In other words, $a_4 = g(r,1) < 0$ when $u_2^* < r$.

By calculating the corresponding Jacobi matrix of $P^*(u^*v^*)$, we obtain

$$T_1 = \frac{1}{1+bv^*} - \frac{2u^*}{r} - \frac{cmv^*}{2\sqrt{u^*}(\sqrt{u^*}+c)^2},$$
$$D_1 = \left(\frac{u^*b}{(1+bv^*)^2} + \frac{m\sqrt{u^*}}{\sqrt{u^*}+c}\right)\left(\frac{\alpha cmv^*}{2\sqrt{u^*}(\sqrt{u^*}+c)^2} - \eta v^*\right).$$

Note that $\frac{u^*b}{(1+bv^*)^2} + \frac{m\sqrt{u^*}}{\sqrt{u^*}+c} > 0$, therefore $D_1 > 0 \iff \frac{\alpha cmv^*}{2\sqrt{u^*}(\sqrt{u^*}+c)^2} - \eta v^*$. Combined with Eq. (3), we calculate and rearrange to obtain $T_1 < 0$ and $D_1 > 0$. It is straightforward to derive the condition $\frac{\eta v^*}{\alpha c} < \frac{mv^*}{2e(e+c)^2} < \frac{e^2}{r(2e+c)}$, which ensures the stability of the positive equilibrium point. □

As shown in Fig. 2, the positive equilibrium shows different stability under the effect of parameter set. In order to explore the fear effect, we will continuously vary the value of b to observe the Hopf bifurcation phenomenon at (u^*,v^*).

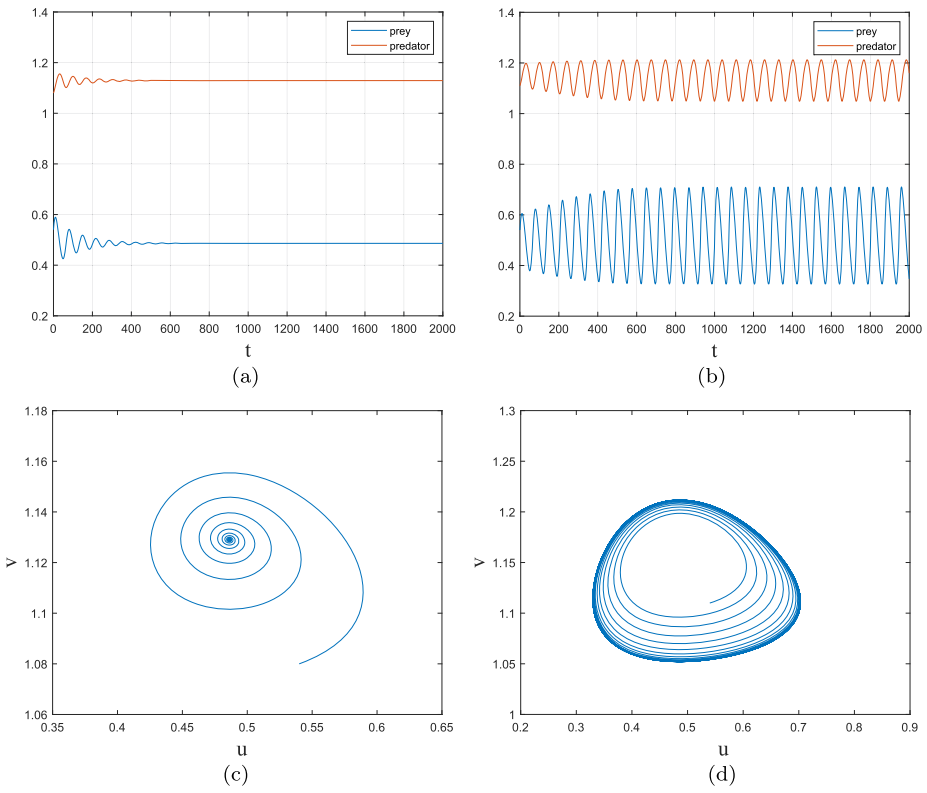

Figure 2 The trajectory portraits of solution of system (2) at (u^*, v^*). It shows (u^*, v^*) is locally asymptotically stable when $r = 2.4(a)(c)$; and there is the stable periodic orbit when $r = 2.59(b)(d)$. Other parameters are $\alpha = 0.78$, $\beta = 0.08$, $\eta = 0.02$, $m = 0.28$, $b = c = 1$

It is well known that $D_1 > 0$ and $T_1 = 0$ are necessary conditions for the occurrence of a Hopf bifurcation. According to formula (8), we rewrite $T_1 = 0$ at $P^*(u^*, v^*)$ as follows:

$$b^* = -\frac{cmrv + 4(u^*)^{\frac{5}{2}} + 4(u^*)^{\frac{3}{2}}c^2 - 2(u^*)^{\frac{3}{2}}r - 2\sqrt{u^*}\,c^2 r - 4u^* cr + 8(u^*)^2 c}{v^*\left(cmv^* r + 4(u^*)^{\frac{3}{2}}c^2 + 8(u^*)^2 c + 4(u^*)^{\frac{5}{2}}\right)}, \tag{10}$$

it can be found that the sign of D_1 at $P^*(u^*, v^*)$ depends on $(\frac{\alpha cm}{2\sqrt{u^*}(\sqrt{u^*}+c)^2} - \eta)v^*$. Thus, we select appropriate parameters to ensure that $\frac{\alpha cm}{2\sqrt{u^*}(\sqrt{u^*}+c)^2}$ is greater than η, and then continuously adjust the value of b to satisfy Eq. (10). As depicted in Fig. 3, $T_1 = 0$ and $\frac{dT_1}{db} < 0$ when $b = b^*$. This leads to $\frac{dRe(\lambda(b))}{db} = \frac{1}{2}\frac{dT_1}{db} \neq 0$, i.e., there are two pure imaginary eigenvalues, $\pm\sqrt{D_1}$, of the matrix $J_{(u^*,v^*)}$. Based on the aforementioned analysis, the system described by Eq. (2) undergoes a supercritical Hopf bifurcation at $b = b^*$ (Fig. 4). This implies that the system transitions from a stable internal equilibrium to a stable limit cycle as b is continuously decreased. We observe that the size of the limit cycle expands as b decreases when $b < b^*$. Conversely, when $b > b^*$, the system described by Eq. (2) is in a stable state, and the steady-state value of the predator diminishes with the escalation of b.

3.2 Stability of equilibrium state for system (1)

To investigate the stability of the equilibrium point of the system under diffusion, a small perturbation $\tilde{u}$ is introduced near the equilibrium point. Specifically, we have $u = u_P + \tilde{u}$,

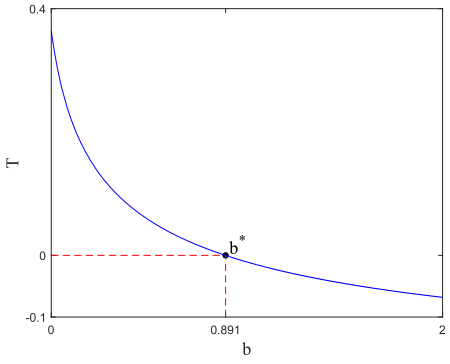

Figure 3 The change of trace T of the Jacobian matrix $J_{(u^*,v^*)}$ when parameter b changes continuously. Other parameters are the same as in Fig. 2(a)

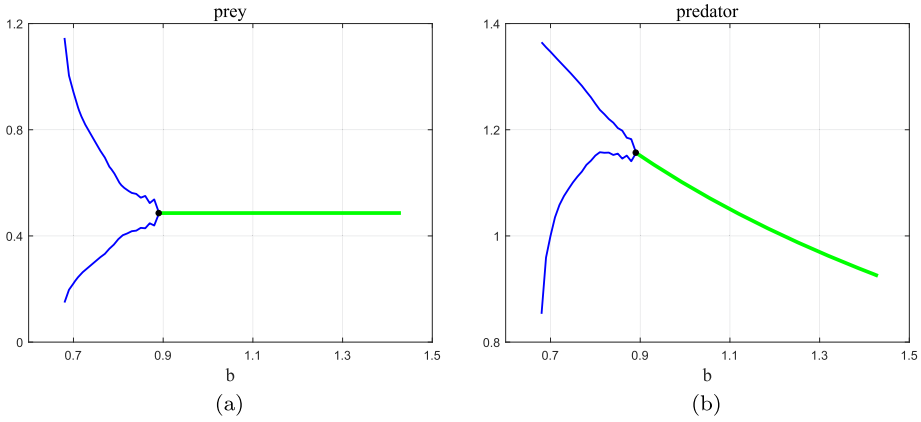

Figure 4 The supercritical Hopf bifurcation about parameters b. The blue line represents the stable limit cycle, and the green line represents a stable equilibrium state. The parameters are the same as in Fig. 2(a)

$v = v_p + \tilde{v}$, where (u_P, v_P) represents any equilibrium point. Then the linearization of (1) at (u_P, v_P) is

$$\begin{bmatrix} \frac{\partial \tilde{u}}{\partial t} \\ \frac{\partial \tilde{v}}{\partial t} \end{bmatrix} = (D\Delta + J_{(u_P,v_P)}) \begin{bmatrix} u \\ v \end{bmatrix}, \tag{11}$$

where $D = \begin{bmatrix} d_1 & 0 \\ 0 & d_2 \end{bmatrix}$. Define the real-valued Sobolev space

$$X = \left\{ (u, v) \in W^{2,2}(\Omega) | \frac{\partial u}{\partial \boldsymbol{n}} = \frac{\partial v}{\partial \boldsymbol{n}} = 0 \ on \ \partial\Omega \right\},$$

and for $U_1 = (u_1, v_1)^T$, $U_2(u_1, v_1)^T \in X$, define the inner product

$$< U_1, U_2 >= \int_\Omega (u_1 v_1 + u_2 v_2) dx.$$

It is well known that the eigenvalue problem

$$-\phi'' = \mu\phi, \ x \in \Omega; \ \phi'(\partial\Omega) = 0,$$

has eigenvalues $\mu_{\boldsymbol{k}} = \boldsymbol{k}^2 > 0$ with corresponding eigenfunction $\phi_{\boldsymbol{k}}(x)$ in the Sobolev space X, where $\begin{cases} \phi_{\boldsymbol{k}}(x) = cos(k_1 x), \\ \boldsymbol{k} = k_1. \end{cases}$ in one-dimensional space and $\begin{cases} \phi_{\boldsymbol{k}}(x) = cos(k_1 x)cos(k_2 x), \\ \boldsymbol{k} = (k_1, k_2). \end{cases}$ in two-dimensional space. Then we consider the solution of Eq. (11) in the following form:

$$\begin{bmatrix} \tilde{u} \\ \tilde{v} \end{bmatrix} = \sum_{k=0}^{\infty} \begin{bmatrix} a_k \\ b_k \end{bmatrix} \phi_{\boldsymbol{k}}(x) e^{\lambda t}, \tag{12}$$

where $a_k, b_k > 0$ are the corresponding small amplitudes, λ represents growth rate of perturbations and x is the spatial coordinates. Equation (12) is a travel wave solution of Eq. (11) if and only if

$$det(J - \boldsymbol{k}^2 D - \lambda I) = 0 \tag{13}$$

holds for some $\boldsymbol{k}$, where $J = \begin{bmatrix} a_{11} & a_{12} \\ a_{21} & a_{22} \end{bmatrix}$, $D = \begin{bmatrix} d_1 & 0 \\ 0 & d_2 \end{bmatrix}$, and I is an identity matrix. Through the analysis of linearization theory, we get the following conclusions.

Theorem 3.2 *For system* (1), (*i*) *the trivial equilibrium* $P_0(0,0)$ *is stable if* $\frac{1}{d_1} < \boldsymbol{k}^2$; (*ii*) $P_1(r,0)$ *is stable if* $\boldsymbol{k}^2 > \frac{g_V(P_1)}{d_2}$; (*iii*) *the positive equilibrium* $P^*(u^*, v^*)$ *is locally stable if it is stable in absence of diffusion.*

Proof Calculate Eq. (13), the corresponding quadratic equations is

$$\lambda^2 - T_2 \lambda + D_2 = 0. \tag{14}$$

The trace T_2 and determinant of the characteristic equation D_2 are respectively:

$$\begin{aligned} T_2 &= T_1 - \boldsymbol{k}^2(d_1 + d_2), \\ D_2 &= D_1 + \boldsymbol{k}^4 d_1 d_2 - k^2(a_{22} d_1 + a_{11} d_2). \end{aligned}$$

By calculating the Jacobian matrix of $P_0(0,0)$, we get $T_2 = 1 - \beta - \boldsymbol{k}^2(d_1 + d_2)$, $D_2 = -\beta + \boldsymbol{k}^4 d_1 d2 - \boldsymbol{k}^2(-\beta d_1 + d_2)$, from $T_2 < 0$,

$$\boldsymbol{k}^2 > \frac{1 - \beta}{d_1 + d_2}, \tag{15}$$

and $D_2 = -\beta + \boldsymbol{k}^4 d_1 d2 - k^2(-\beta d_1 + d_2) = (\boldsymbol{k}^2 d_1 - 1)(\beta + \boldsymbol{k}^2 d_2)$, therefore $D_2 > 0$ is determined by

$$\boldsymbol{k}^2 > \frac{1}{d_1}. \tag{16}$$

Considering Eq. (15) and Eq. (16), it is concluded that $P_0(0,0)$ is stable if $\frac{1}{d_1} < \boldsymbol{k}^2$. Similarly, at equilibrium point $P_1(r,0)$, we set

$$\begin{aligned} T_2 &= -1 + a_{22} - \boldsymbol{k}^2(d_1 + d_2) < 0, \\ D_2 &= -a_{22} + \boldsymbol{k}^4 d_1 d_2 - \boldsymbol{k}^2(a_{22} d_1 - d_2) > 0. \end{aligned} \tag{17}$$

The condition $\boldsymbol{k}^2 > \frac{a_{22}}{d_2}$ can be easily obtained by simplifying Eq. (17). Moreover, a_{22} is less than 0 when $r \in (0, u_1^*) \cup (u_2^*, \infty)$, which means Eq. (17) is always true.

Next, we consider the stability of $P^*(u^*, v^*)$. Assuming it is stable in the absence of diffusion, that is, $T_1 = a_{11} + a_{22} = a_{11} < 0$ and $D_1 = a_{11}a_{22} - a_{12}a_{21} = -a_{12}a_{21} > 0$, thus $T_2 = T_1 - \boldsymbol{k}^2(d_1 + d_2) < 0$. It is apparent that the positive equilibrium will be unstable when $D_2 < 0$, but because of $a_{11} < 0$ and $a_{22} = 0$,

$$D_2 = D_1 + \boldsymbol{k}^4 d_1 d_2 - \boldsymbol{k}^2(a_{22}d_1 + a_{11}d_2) > 0,$$

which means the positive equilibrium $P^*(u^*, v^*)$ is locally stable during diffusion. □

Remark 3.3 We have found that system (2) will not undergo instability caused by diffusion around $P^*(u^*, v^*)$. That is to say, the Turing pattern cannot be observed in this model.

In the following, we shall discuss the existence of Hopf bifurcations and steady state bifurcations in the diffusion system (1). At the coexistence equilibrium $P^*(u^*, v^*)$, T_2 and D_2 are expressed as

$$T_2 = \frac{1}{1 + bv^*} - \frac{2u^*}{r} - \frac{cmv^*}{2\sqrt{u^*}(\sqrt{u^*} + c)^2} - \boldsymbol{k}^2(d_1 + d_2), \tag{18}$$

$$\begin{aligned} D_2 = {} & \left(\frac{u^* b}{(1 + bv^*)^2} + \frac{m\sqrt{u^*}}{\sqrt{u^*} + c}\right)\left(\frac{\alpha cmv^*}{2\sqrt{u^*}(\sqrt{u^*} + c)^2} - \eta v^*\right) \\ & + \boldsymbol{k}^4 d_1 d_2 - \boldsymbol{k}^2 d_2 \left(\frac{1}{1 + bv^*} - \frac{2u^*}{r} - \frac{cmv^*}{2\sqrt{u^*}(\sqrt{u^*} + c)^2}\right), \end{aligned} \tag{19}$$

respectively. It is obvious that $T_2 < 0, D_2 > 0$ if $b > b^*$, which means that system (1) is always stable, where b^* is defined by Eq. (10). We take parameters b and d_2 as variables, rewriting $T_2 = 0$ as

$$L_k : d_2 = d_{2L}(b, \boldsymbol{k}) \tag{20}$$

and $D_2 = 0$ as

$$Z_k : d_2 = d_{2Z}(b, \boldsymbol{k}). \tag{21}$$

Setting $\frac{\alpha cm}{2\sqrt{u^*}(\sqrt{u^*}+c)^2} > \eta$ and combining (20) with (21), then the two curves L_k, Z_k intersect at (b_k^*, d_{2k}^*), where

$$b_k^* = \frac{2r\sqrt{u^*}(\sqrt{u^*} + c)^2(1 - k^2 d_1 - k^2 d_2) - 4u\sqrt{u^*}(\sqrt{u^*} + c)^2 - cmvr}{v\left[2r\sqrt{u^*}(\sqrt{u^*} + c)^2(k^2 d_1 + k^2 d_2) + 4u\sqrt{u^*}(\sqrt{u^*} + c)^2 + cmvr\right]}, \quad d_{2k}^* = \frac{\sqrt{a_{21}a_{12}}}{\boldsymbol{k}^2}. \tag{22}$$

If $b > b_k^*$, $\frac{dT_1(b)}{db} \neq 0$, then system (1) undergoes steady state bifurcations on line L_k and Hopf bifurcations on line H_k around the equilibrium $P^*(u^*, v^*)$ for $\boldsymbol{k}^2 = 0, 1, \ldots, \boldsymbol{k^*} = \left[\frac{a_{11}}{d_1 + d_2}\right]$, where $[\cdot]$ stands for the integer part function.

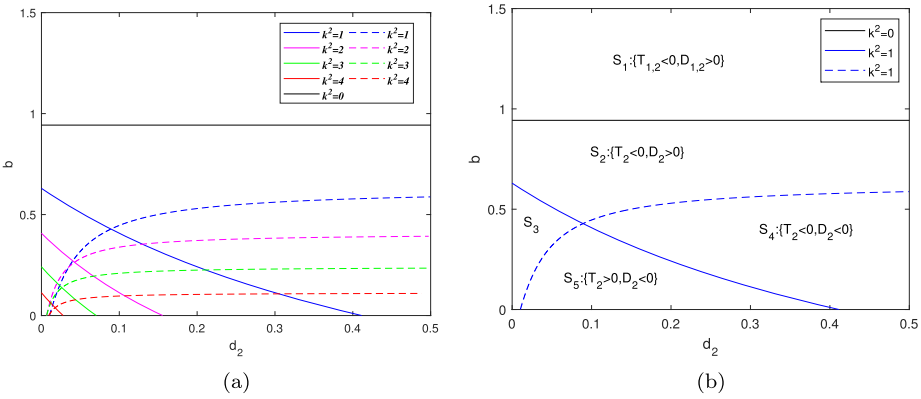

Figure 5 Bifurcation diagram of model (1) in the $d_2 - b$ plane. The solid line represents H_k, and the dotted line represents L_k. Here $d_1 = 0.1$, the other parameters are the same as in Fig. 2(a)

4 Numerical simulation

In this paper, we performed numerical simulations of ODE model (2) and partial differential model (1). We first show two states of system (2) when environmental capacity r takes different values in Fig. 2. Around the positive equilibrium point, we see stable solution trajectory when $r = 2.4 < r* = 2.49$ and a stable periodic orbit when $r = 2.59 > r* = 2.49$. Then we continuously change the value of parameter b in order to explore the bifurcation condition. Under the premise of selecting the appropriate parameters, we found that system (2) undergoes a supercritical Hopf bifurcation at $b^* = 0.89$ (see Fig. 4). When $b < b^*$, a stable limit cycle is generated and the radius of the limit cycle increases with the decrease of b. When b gradually increases from b^*, the equilibrium value of prey species remains constant but the equilibrium value of predator species decreases. Through the analysis of the relation of d_2 and b, there are Hopf bifurcations and steady state bifurcations on H_k, L_k, respectively. As shown in Fig. 5, S_1, S_2 represent the stable space and S_3, S_4, S_5 are the unstable space. H_0 will not intersect with $L_{\boldsymbol{k}}$ for any $\boldsymbol{k} > 0$, which verifies that there is no diffusion-driven instability.

In nature, due to factors such as resources and competition, organisms have a tendency to spread to areas with low population density. Next we used the finite difference method and the finite element approximation to simulate system (1), respectively.

4.1 Finite-difference method

First, we establish a grid on the interval $\Omega = [0, X]$ with evenly spaced points x_i ($i = 0, 1, 2, \ldots, N$) in one-dimensional space, the space step $h = \frac{X}{N}$, and $x_i = ih$. For two-dimensional space, take a square grid on $\Omega = [0, X] \times [0, Y]$ with grid points $(x_i, y_j) = (ih, jh)$, $i, j = 0, 1, 2, \ldots, N$. Similarly, we divide time interval $[0, T]$ evenly into M parts, so that time step $\triangle t = \frac{T}{M}$ and $t_m = m \triangle t$, $m = 0, 1, 2, \ldots, M$.

The forward difference is used in time dimension, and the central difference is used in one-dimensional space and in two-dimensional space to approximate the Laplacian re-

spectively.

$$\frac{\partial U^m}{\partial t} = \frac{U^m - U^{m-1}}{\triangle t},$$
$$\Delta U_i = \frac{(U_{i+1} + U_{i-1} - 2U_i)}{h^2},$$
$$\Delta U_{i,j} = \frac{(U_{i+1,j} + U_{i-1,j} + U_{i,j-1} + U_{i,j+1} - 4U_{i,j})}{h^2}.$$

The difference format for the predator population V is the same as that of U above. Then the general form of difference equation in one-dimensional space is as follows:

$$\begin{aligned} \frac{\partial U_i^m}{\partial t} &= f(U_i^{m-1}) + \Delta U_i^m, \\ \frac{\partial V_i^m}{\partial t} &= f(V_i^{m-1}) + \Delta V_i^m, \end{aligned} \tag{23}$$

where U_i^m, V_i^m are the approximation of $u(x,t), v(x,t)$ at position ih at time t_m, $i = 0,1,2,\ldots,N$, and $m = 1,2,3,\ldots,M$. And the nonnegative initial condition

$$U_i^0 = u(ih,0), \quad V_i^0 = v(ih,0).$$

The following is the general form of difference equation in two-dimensional space

$$\begin{aligned} \frac{\partial U_{i,j}^m}{\partial t} &= f(U_{i,j}^{m-1}) + \Delta U_{i,j}^m, \\ \frac{\partial V_{i,j}^m}{\partial t} &= f(V_{i,j}^{m-1}) + \Delta V_{i,j}^m, \end{aligned} \tag{24}$$

where $i = 0,1,2,\ldots,N$ and $m = 1,2,3,\ldots,M$. The nonnegative initial condition

$$U_{i,j}^0 = u([ih,jh],0), \quad V_{i,j}^0 = v([ih,jh],0).$$

Both of the above difference equations are used the homogeneous Neumann boundary conditions, which means zero-flux boundary, therefore the outflow and inflow at the edge of the grid are set to 0 in the difference program.

We have simulated its diffusion in one-dimensional space and two-dimensional space successively. Firstly, it is assumed that the density distribution at the initial time in one-dimensional space is uniform in Fig. 6, we take five different values of r. Figure 6$(a)(b)$ show the system quickly and smoothly close to internal equilibrium when $r = 1$, it remains stable when r increases to 2. But prey and predator begin to fluctuate with time when $r = 2.3$, it can be found that the fluctuation amplitude gradually decreases with time and finally tends to be balanced. At $r = 2.6$, the population densities begin to fluctuate greatly and periodically. If r increases to 6, the prey population reaches its maximum, and the predator goes to extinction gradually, that means the system goes to the predator-free equilibrium $P_1(r,0)$. From Fig. 6, with the increase of r, system (1) becomes unstable at internal equilibrium P^*, finally ends up at boundary balance.

Figure 7 shows the spatial distribution of system (1) under nonuniform initial value. Assuming that the area is closed, the species will not go out of this area, nor will they

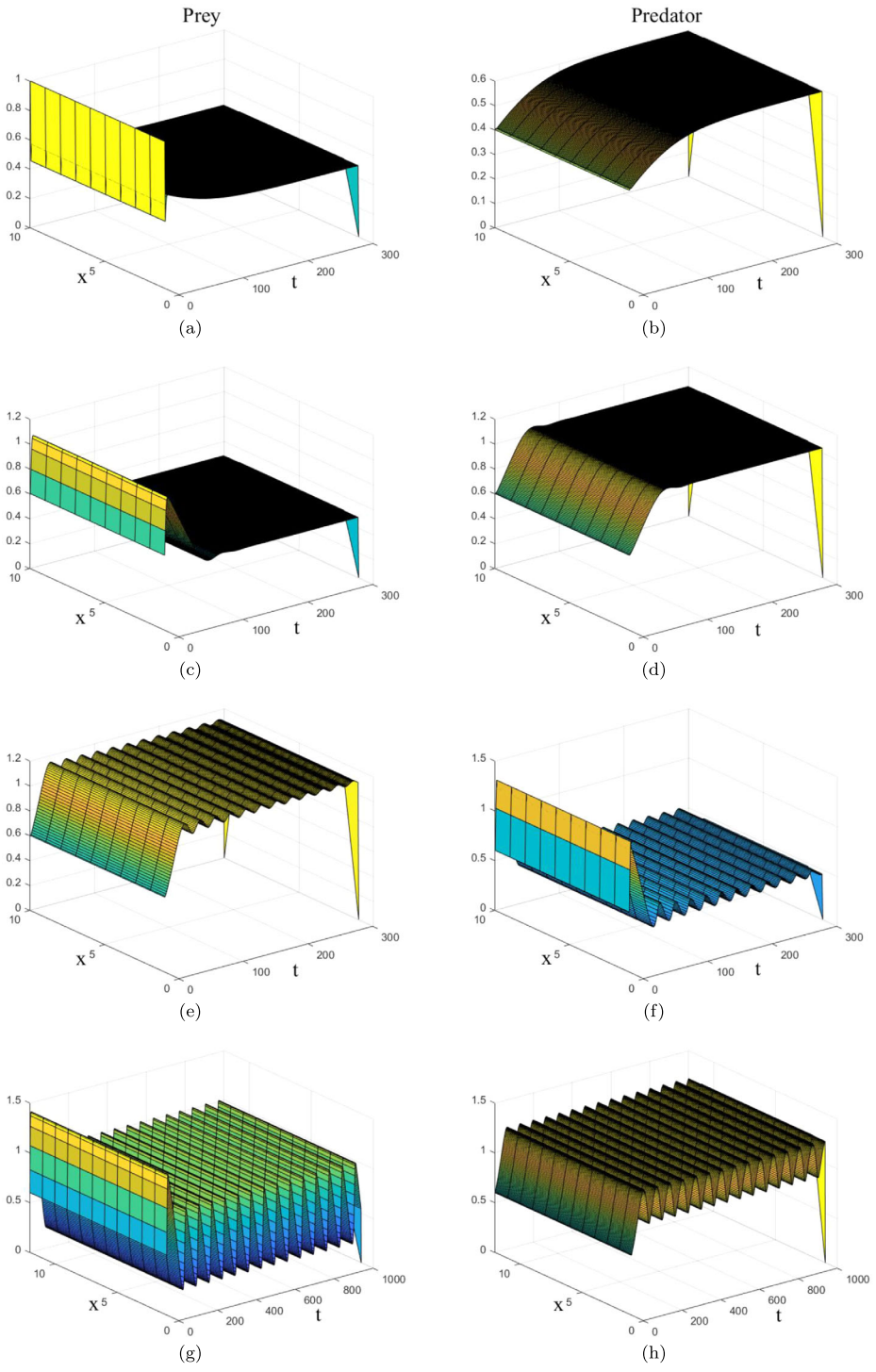

Figure 6 The spatial distribution of predators and prey in one-dimensional simulated diffusion, the left column ((a)to(i)) on behalf of the prey and the right column ((b)to(j)) on behalf of the predator. Here the initial spatial distribution is assumed to be uniform. Both prey and predator populations are stable for $r = 1$ (a)(b); remain stable for $r = 2$ (c)(d); a gradually decreasing oscillation occurs for $r = 2.3$ (e)(f); steady large amplitude oscillation for $r = 2.6$; when r increases to 6 (i)(j), the predator-free equilibrium $P_1(r, 0)$ is stable

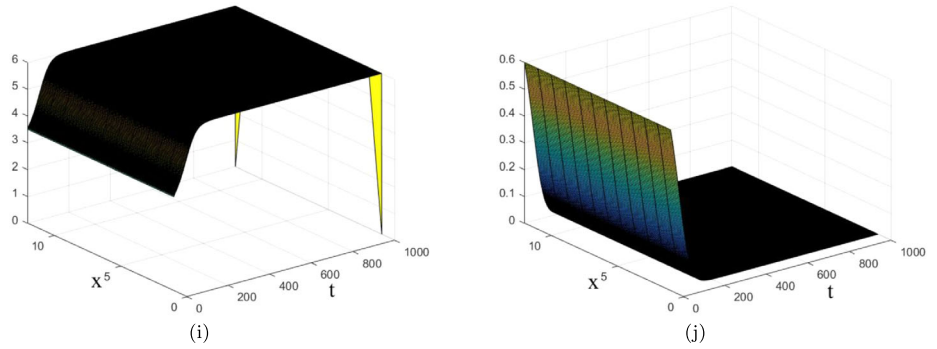

Figure 6 Continued

come in from outside the area. And the homogeneous Neumann boundary condition is used at the boundary. Here, we take the initial condition

$$u(x,0) = u^* + 0.2sin(\frac{\pi}{6}x),$$
$$v(x,0) = v^* - 0.1sin(\frac{\pi}{6}x).$$

We choose four different values of diffusion velocity to simulate the diffusion of predator and prey. It is easy to find that the system is always stable when the species diffuses at different speeds. It can be seen from Fig. 7(a)(b) to Fig. 7(g)(h) that different regions have different amplitudes of stationary shocks and the amplitude decreases with time. When d_1 and d_2 gradually increase, the amplitude difference in different regions decreases at a faster rate.

Figure 8 simulates the reaction–diffusion of system (1) in the two-dimensional rectangular region, meanwhile the parameters we selected can make the ODE system have stable positive equilibrium. The results show that the spatial distribution tends to be uniform with the increase of time t_m and continue to increase T. It can be found that the pattern almost no longer changes when $T = 100$.

4.2 Finite element method

Before giving the complete approximation scheme, we introduce some preparation steps. Let $\varpi^h = \{\tau \mid \textit{Compact approximately equilateral nonoverlapping closed triangles}\}$ be a partition of the domain Ω, h_τ denotes the length of the longest side of triangle τ, and $h = max\, h_\tau$. We assume that h is small enough, that is, the partition of ϖ^h to domain Ω is sufficiently detailed; therefore, we ignore the error and study the problem in the approximate region Ω_h. Define piecewise linear continuous function space

$$F^h := \{f \in C(\Omega_h) \mid f \textit{ is linear on each } \tau\}.$$

Let $\varphi_1, \varphi_2, \ldots, \varphi_n$ be the basis functions of F^h and $x_1, x_2, \ldots, x_n$ represent n nodes in Ω_h, that is, the vertices of all triangles. $0 \leq \varphi_i(x) \leq 1$ denotes the weight distribution of the node x_i, and necessarily $\varphi_i(x_k) = \delta_{ik}$ is the Kronecker delta function. Thus, for any function

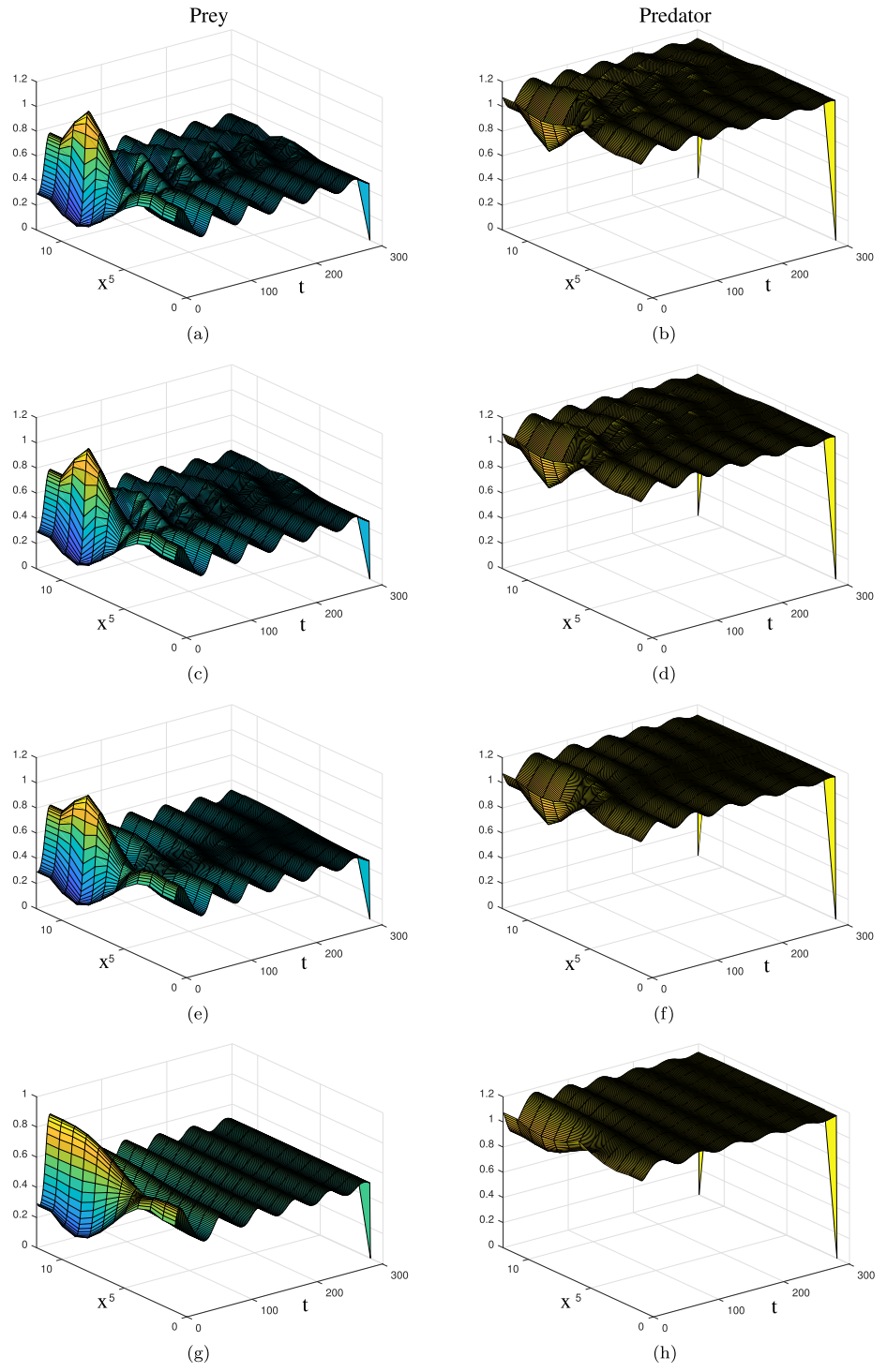

Figure 7 The spatial distribution of predator and prey in one-dimensional diffusion under heterogeneous initial values. The left column ((a)to(g)) on behalf of the prey and the right column ((b)to(h)) on behalf of the predator. We take different values of diffusion parameter d to observe the influence of diffusion efficiency on the system. $d_1 = d_2 = 1$ represent tiny diffusion in $(a)(b)$, $d_1 = d_2 = 10$ in $(c)(d)$, $d_1 = d_2 = 10^2$ in $(e)(f)$, and $d_1 = d_2 = 10^3$ in $(g)(h)$. We take $r = 2.34$ and other parameters are the same as in Fig. 2, which means system (2) has a positive equilibrium

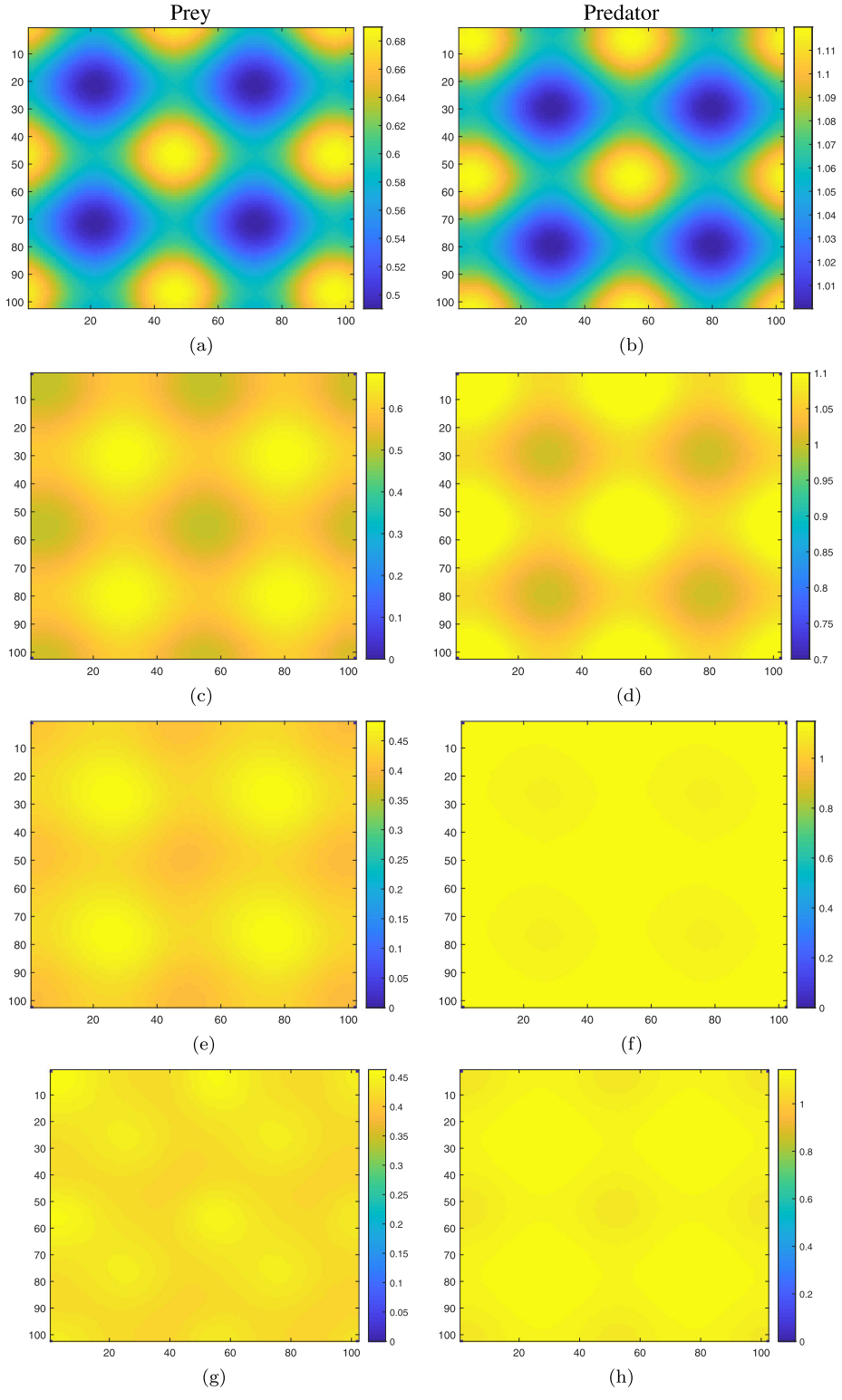

Figure 8 The spatial distribution of predators and prey in two-dimensional diffusion. The left column ((a)to(g)) on behalf of the prey and the right column ((b)to(h)) on behalf of the predator. (*a*)(*b*) $T = 1$; (*c*)(*d*) $T = 20$; (*e*)(*f*) $T = 50$; (*g*)(*h*) $T = 100$, Here $d_1 = d_2 = 30$, other parameters are the same as in Fig. 2(a)

$f \in F^h$, it can be expressed by the combination of node value and weight function

$$f(\boldsymbol{x}) = \sum_{i=1}^{n} \varphi_i(\boldsymbol{x}) f(x_i). \tag{25}$$

And we define the following matrix:

$$\begin{aligned} &M_{ii} := \int_{\Omega} \varphi_i \, d\boldsymbol{x}, \\ &K_{ij} := \int_{\Omega} \nabla \varphi_i \cdot \nabla \varphi_j \, d\boldsymbol{x}, \\ &L_{ij} := M_{ii}^{-1} K_{ij}. \end{aligned} \tag{26}$$

Then we introduce the discrete finite element method and equations derivation. Divide the time interval $[0, T]$ evenly into M parts, so that time step $\triangle t = \frac{T}{M}$ and $t_m = m \triangle t$, $m = 0, 1, 2, \ldots, M$; we define the discrete reaction from approximation of Eq. (2)

$$\begin{aligned} h_1(U^m, U^{m-1}, V^m, V^{m-1}) &= U^m \left(\frac{1}{1 + bV^{m-1}} - \frac{U^{m-1}}{r}\right) - \frac{m\sqrt{U^{m-1}}}{\sqrt{U^{m-1}} + c} V^m, \\ h_2(U^{m-1}, V^m) &= -\beta V^m + \frac{\alpha m \sqrt{U^{m-1}}}{\sqrt{U^{m-1}} + c} V^m - \eta U^{m-1} V^m, \end{aligned} \tag{27}$$

where U^m, V^m are the approximations of population u, v at time t_m.

Let $U_i^m = U^m(x_i)$ and $V_i^m = V^m(x_i)$, $i = 1, 2, \ldots, n$, under the homogeneous Neumann boundary condition, we have the discrete form of the reaction–diffusion equation:

$$\begin{aligned} \frac{U_i^m - U_i^{m-1}}{\triangle t} + d_1 \sum_{j=1}^{n} K_{ij} U_j^m &= M_{ii} h_1, \\ \frac{V_i^m - V_i^{m-1}}{\triangle t} + d_2 \sum_{j=1}^{n} K_{ij} V_j^m &= M_{ii} h_2. \end{aligned} \tag{28}$$

Multiplying both equations by $\triangle t \, (M)^{-1}$, we obtain

$$\begin{aligned} (U_i^m - U_i^{m-1}) M^{-1} + d_1 \triangle t M^{-1} \sum_{j=1}^{n} K_{ij} U_j^m &= \triangle t \, h_1, \\ (V_i^m - V_i^{m-1}) M^{-1} + d_2 \triangle t M^{-1} \sum_{j=1}^{n} K_{ij} V_j^m &= \triangle t \, h_1. \end{aligned} \tag{29}$$

Combining Eqs. (26), (27) and merging the terms, Eq. (29) can be rewritten as

$$\begin{aligned} &A^{m-1} U^m + B^{m-1} V^m = U^{m-1}, \\ &C^{m-1} V^m = V^{m-1}, \end{aligned} \tag{30}$$

where

$$U^m{}_i = U^m(x_i),\ V^m{}_i = V^m(x_i),$$

$$U^0(x_i) = u_0(x_i),\ V^0(x_i) = v_0(x_i),$$

$$A^{m-1} = I + (d_1 L - \Theta_3 + \frac{1}{r}\Theta_1)\ \triangle t,$$

$$B^{m-1} = m\,\Theta_2\ \triangle t,$$

$$C^{m-1} = I + (d_2 L + \beta - \alpha m \Theta_2 + \eta \Theta_1)\ \triangle t,$$

$$\Theta_1 = diag\left\{U^{m-1}(x_1), U^{m-1}(x_2), \ldots, U^{m-1}(x_n)\right\},$$

$$\Theta_2 = diag\left\{\frac{\sqrt{U^{m-1}(x_1)}}{\sqrt{U^{m-1}(x_1)}+c}, \frac{\sqrt{U^{m-1}(x_2)}}{\sqrt{U^{m-1}(x_2)}+c}, \ldots, \frac{\sqrt{U^{m-1}(x_n)}}{\sqrt{U^{m-1}(x_n)}+c}\right\},$$

$$\Theta_3 = diag\left\{\frac{1}{1+b\,V^{m-1}(x_1)}, \frac{1}{1+b\,V^{m-1}(x_2)}, \ldots, \frac{1}{1+b\,V^{m-1}(x_n)}\right\}.$$

Next, we define a two-dimensional simulation region and iterate Eq. (30) under two different initial values, then obtain Fig. 9 and Fig. 10. The parameter values of the two figures are $\alpha = 0.78$, $\beta = 0.1$, $\eta = 0.05$, $m = 0.25$, $b = 1$, $c = 5$, $r = 4$, $d_1 = d_2 = 1$. In Fig. 9, we choose the initial value of the binary trigonometric function for the density distribution of both predator and prey (see Fig. 9(*a*)(*b*)). With the increase of time, the pattern gradually becomes irregular under the effect of diffusion. In general, the distribution of species density fluctuates around the equilibrium point, particularly, the prey forms ring structures (Fig. 9(*e*)(*g*)). In fact, this also reflects the change of species density in different areas due to the change of environmental resources and predation. Then, let the initial value of prey remain unchanged and the initial value of predator use an approximate normal distribution centered on the lakes (Fig. 10(*a*)(*b*)). As a result of chasing and predation, the distribution of predator and prey shows a certain correlation. Through the snapshots in Fig. 10, it can be found that the area where predator density is concentrated gradually decreases over time; at the same time, prey is concentrated in areas with relatively low predator density. And after a while, the number of predators increases again in areas with higher prey populations. Through the above figures, it can be verified that although diffusion affects the spatial distribution of the population, it will not change the stability at P^*.

5 Conclusion and discussion

In this paper, a diffusive predator–prey interaction mathematical model has been developed. Observations of grassland social animals have revealed that stronger prey individuals will encircle and protect the weaker members in the center to avoid predation, indicating that they have a certain level of aggression. To account for this anti-predation behavior, the model takes the square root of the prey population in response function and adds the predator's loss term. Within a certain range of η, the equilibrium value of the prey becomes higher. Besides, considering the presence of predators can lead to a decline in prey birth rates, we include the fear effect in the model. The stability of the equilibrium point in the case of diffusion and non-diffusion is analyzed by the linearization method respectively. We give the conditions for the stability of the internal equilibrium point of the

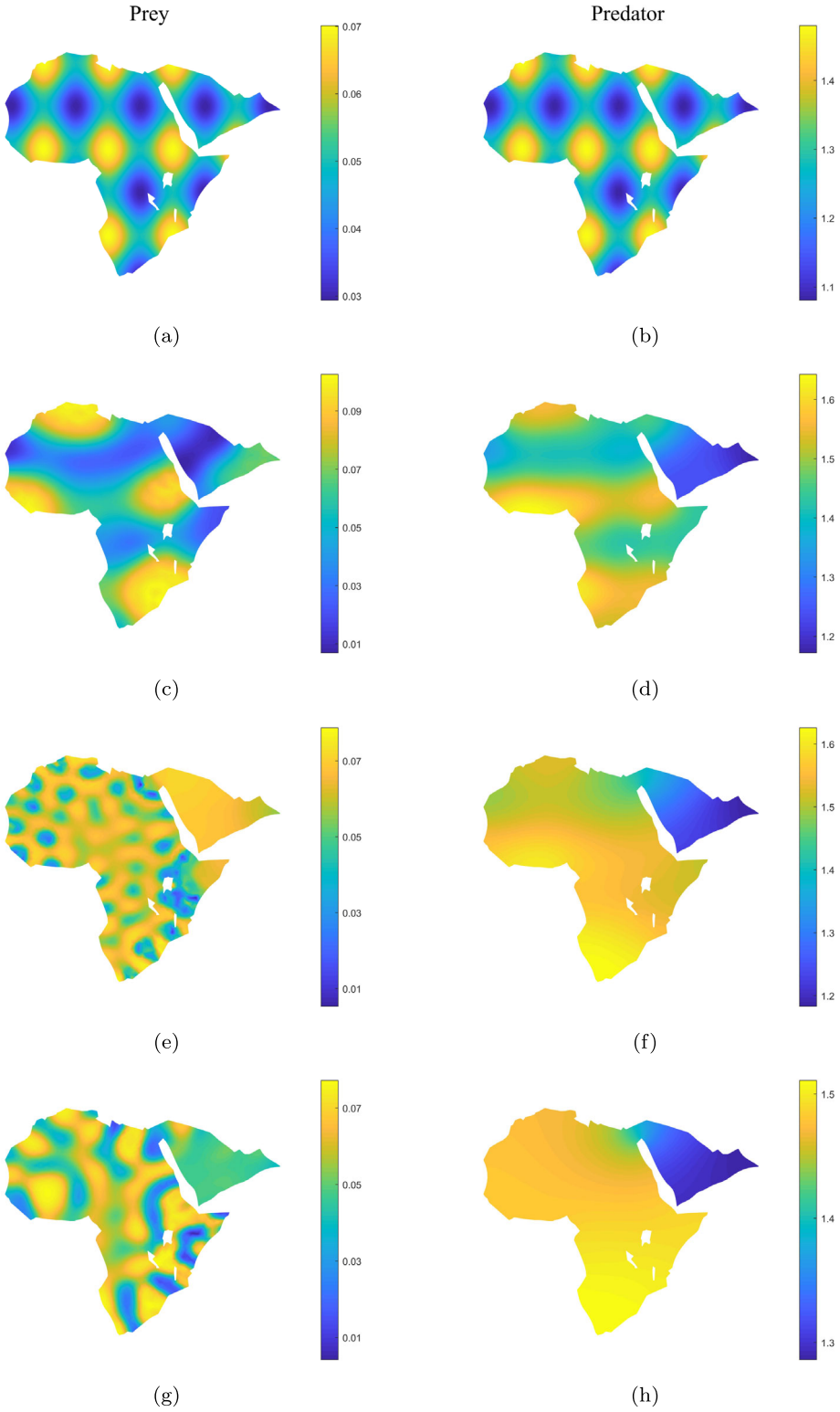

Figure 9 The variation profiles of the species population at different times. The left column ((a)to(g)) on behalf of the prey and the right column ((b)to(h)) on behalf of the predator. Here, $\Delta t = 1$, (*a*)(*b*) $T = 30$; (*c*)(*d*) $T = 80$; (*e*)(*f*) $T = 130$; (*g*)(*h*) $T = 200$

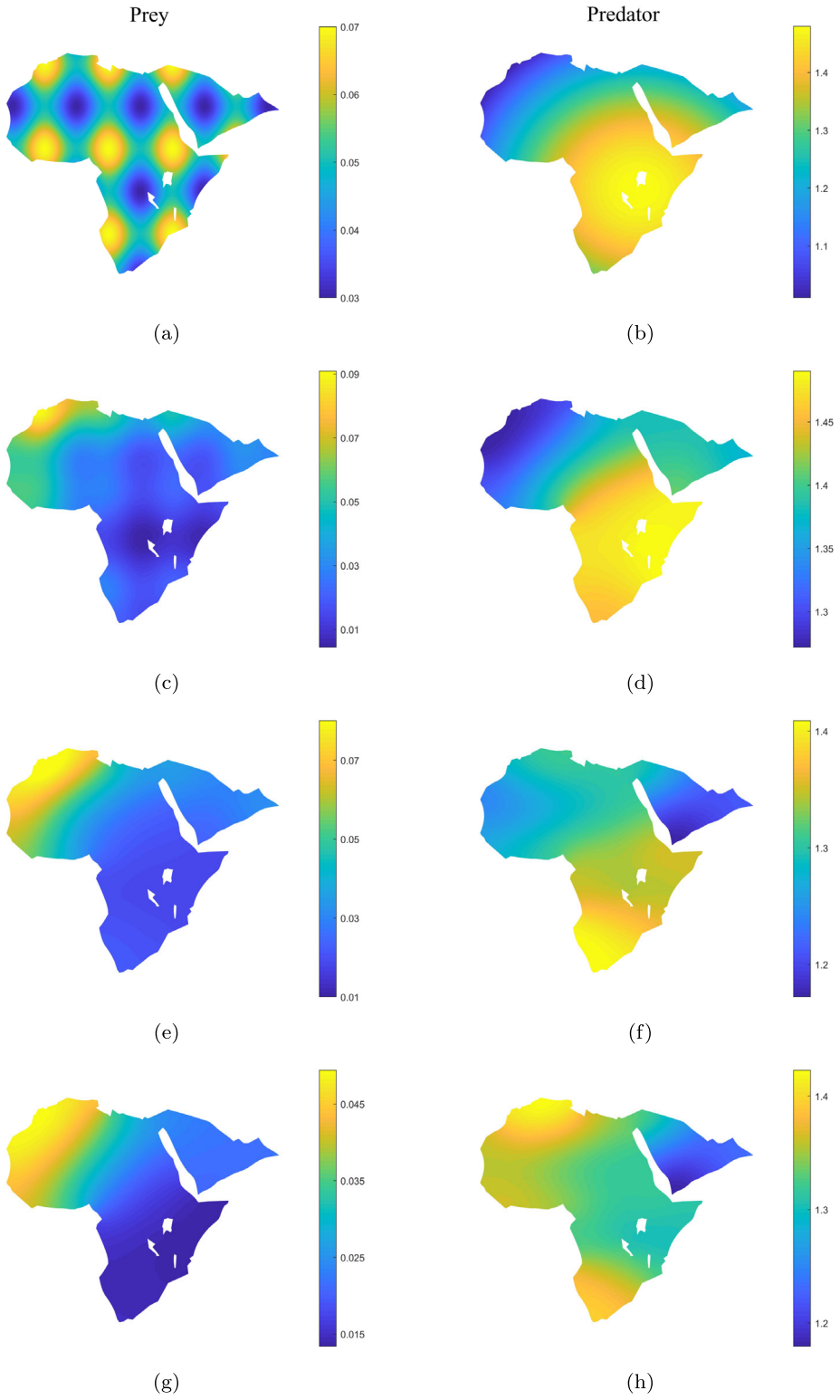

Figure 10 The variation profiles of the species population at different times. The left column ((a)to(g)) on behalf of the prey and the right column ((b)to(h)) on behalf of the predator. Here, $\Delta t = 1$, (*a*)(*b*) $T = 30$; (*c*)(*d*) $T = 80$; (*e*)(*f*) $T = 130$; (*g*)(*h*) $T = 200$

non-diffusion system, the results show that the Turing pattern through diffusion-driven instability cannot be generated in this model, that is, the number of the two species will still remain a uniform steady state during the process of spatial diffusion and interaction. Then we have made a bifurcation analysis of the parameter b, after some other parameters are given, the supercritical Hopf bifurcation occurs at b^* and the results show that the fear effect makes it more difficult for predators to hunt by affecting the birth of prey; in other words, the higher the cost of prey to evade predation, the lower the population level of predators in the coexistence equilibrium. Finally, we perform numerical simulation by MATLAB. We use the finite difference method in a rectangular region and the finite element approximation in irregular regions to simulate the diffusion system (1), respectively. The reaction–diffusion system has more abundant phenomena than the ODE system, and spatial dynamic behaviors such as smooth oscillations, fluctuations, and fringes can be observed under different given parameters and initial values. It can be found that the changes of spatial patterns in customized irregular regions are complex and diverse, and the patch pattern is significantly affected by the difference of interval division; therefore, the error can be reasonably reduced by using sufficiently fine triangular elements to approximate.

Acknowledgements
The authors would like to thank the editor and the anonymous reviewers for their constructive comments and suggestions to improve the quality of the paper.

Author contributions
All authors read and approved the final manuscript.

Funding
This work is supported by the National Natural Science Foundation of China (Grant Nos.12361100, 12201086) and the Chongqing Education Commission Youth Project (Grant No. KJQN202201209).

Data availability
The data used and analyzed during the current study are available on reasonable request.

Declarations

Ethics approval and consent to participate
Not applicable.

Competing interests
The authors declare no competing interests.

Author details
[1]School of Mathematics and Statistics, Hubei Minzu University, Enshi 445000, Hubei, China. [2]College of Computer Science and Engineering, Chongqing Three Gorges University, Wanzhou 404100, Chongqing, China.

Received: 25 July 2024 Accepted: 12 January 2025 Published online: 03 February 2025

References

1. Lotka, A.J.: Elements of mathematical biology. Elements of Physical Biology (1925)
2. Volterra, V.: Variazione e fluttuazini del numero dindividui in specie an imali conviventi. Atti R. Accad. Naz. Lincei, Mem. Cl. Sci. Morali Stor. Filol. **2**, 31–113 (1926)
3. Holling, C., Stanley, C.: The functional response of invertebrate predators to prey density. Mem. Entomol. Soc. Can. **98**(S48), 5–86 (1966)
4. Tian, Y., Weng, P.: Stability analysis of diffusive predator-prey model with modified Leslie-Gower and Holling-type II schemes. Acta Appl. Math. **114**, 173–192 (2011)
5. Liu, Z., Zhong, S., Yin, C., Chen, W.: Dynamics of impulsive reaction–diffusion predator–prey system with Holling type III functional response. Appl. Math. Model. **35**, 5564–5578 (2011)
6. Feng, J., Zhao, Z.: Stability analysis of discrete-time multi-patch Beddington–deAngelis type predator-prey model with time-varying delay. Adv. Differ. Equ. **2019**, 444, 1–12 (2019)
7. Haque, M.: A detailed study of the Beddington–deAngelis predator–prey model. Math. Biosci. **234**, 1–16 (2011)
8. Li, X., Dong, J.: Complicate dynamical properties of a discrete slow-fast predator-prey model with ratio-dependent functional response. Sci. Rep. **13**, 20575 (2023)

9. Zhang, F., Li, Y.: Stability and Hopf bifurcation of a delayed-diffusive predator–prey model with hyperbolic mortality and nonlinear prey harvesting. Nonlinear Dyn. **88**, 1397–1412 (2017)
10. Kumari, N., Mohan, N.: Cross diffusion induced Turing patterns in a tritrophic food chain model with Crowley-Martin functional response. Mathematics **7**, 229 (2019)
11. Ajraldi, V., Pittavino, M., Venturino, E.: Modeling herd behavior in population systems. Nonlinear Anal., Real World Appl. **12**, 2319–2338 (2011)
12. Braza, P.A.: Predator–prey dynamics with square root functional responses. Nonlinear Anal., Real World Appl. **13**, 1837–1843 (2012)
13. Tang, X., Song, Y.: Bifurcation analysis and Turing instability in a diffusive predator-prey model with herd behavior and hyperbolic mortality. Chaos Solitons Fractals **81**, 303–314 (2015)
14. Panja, P.: Combine effects of square root functional response and prey refuge on predator–prey dynamics. Int. J. Model. Simul. **41**, 1–8 (2020)
15. Prasad, K.D., Prasad, B.S.R.V.: Qualitative analysis of additional food provided predator–prey system with anti-predator behaviour in prey. Nonlinear Dyn. **96** 1765–1793 (2019)
16. Cresswell, W.: Predation in bird populations. J. Ornithol. **152**, 251–263 (2011)
17. Peacor, S.D., Peckarsky, B.L., Trussell, G.C. et al.: Costs of predator-induced phenotypic plasticity: a graphical model for predicting the contribution of nonconsumptive and consumptive effects of predators on prey. Oecologia **171**, 1–10 (2013)
18. Creel, S., Christianson, D.: Relationships between direct predation and risk effects. Trends Ecol. Evol. **23**, 194–201 (2007)
19. Lima, L.S.: Predators and the breeding bird: behavioral and reproductive flexibility under the risk of predation. Biol. Rev. Camb. Philos. Soc. **84**, 485–513 (2009)
20. Zanette, L.Y., White, A.F., Allen, M.C., Clinchy, M.: Perceived predation risk reduces the number of offspring songbirds produce per year. Science **334**, 1398–1401 (2011)
21. Wang, X., Zanette, L., Zou, X.: Modelling the fear effect in predator-prey interactions. Math. Biol. **73**, 1179–1204 (2016)
22. Duan, D., Niu, B., Wei, J.: Hopf-Hopf bifurcation and chaotic attractors in a delayed diffusive predator-prey model with fear effect. Chaos Solitons Fractals **123**, 206–216 (2019)
23. Samaddar, S., Dhar, M., Bhattacharya, P.: Effect of fear on prey-predator dynamics: exploring the role of prey refuge and additional food. Chaos **30**, 063129 (2020)
24. Liu, F., Du, Y.: Spatiotemporal dynamics of a diffusive predator-prey model with delay and Allee effect in predator. Math. Biosci. Eng. **20**(11), 19372–19400 (2023)
25. Turing, A.: The chemical basis of morphogenesis. Philos **237**, 37–72 (1952)
26. Segel, L., Jackson, J.: Dissipative structure: an explanation and an ecological example. J. Theor. Biol. **37**, 545–559 (1972)
27. Chakraborty, B., Bairagi, N.: Complexity in a prey-predator model with prey refuge and diffusion. Ecol. Complex. **37**, 11–23 (2019)
28. Guin, L.N.: Spatial patterns through Turing instability in a reaction–diffusion predator–prey model. Math. Comput. Simul. **109**, 174–185 (2015)
29. Souna, F., Lakmeche, A., Djilali, S.: Spatiotemporal patterns in a diffusive predator-prey model with protection zone and predator harvesting. Chaos Solitons Fractals **140**, 110180 (2020)
30. Guin, L.N., Haque, M., Mandal, P.K.: The spatial patterns through diffusion-driven instability in a predator–prey model. Appl. Math. Model. **36**(5), 1825–1841 (2012)
31. Chen, S., Shi, J.: Global stability in a diffusive Holling–Tanner predator–prey model. Appl. Math. Lett. **25**(3), 614–618 (2012)
32. Fang, Q., Cheng, H., Yuan, R.: Spatial dynamics of some modified Leslie-Gower prey-predator model with shifting habitat. J. Math. Anal. Appl. **518**, 126713 (2023)
33. Alkhasawneh, R.A.: A new stage structure predator-prey model with diffusion. Int. J. Appl. Comput. Math. **7**, 113 (2021)
34. Zheng, P.: On a two-species competitive predator-prey system with density-dependent diffusion. Math. Biosci. Eng. **19**(12), 13421–13457 (2022)
35. Chakraborty, B., Ghorai, S., Bairagi, N.: Reaction-diffusion predator-prey-parasite system and spatiotemporal complexity. Appl. Math. Comput. **386**, 125518 (2020)

Publisher's Note